applied sciences

MDPI

Article

Optimization of Silicon MZM Fabrication Parameters for High Speed Short Reach Interconnects at 1310 nm

Alexis Abraham [1], Thomas Anfray [1], Olivier Dubray [1], Daivid Fowler [1], Ségolène Olivier [1], Delphine Marris-Morini [2] and Benoit Charbonnier [1,*]

[1] Commissariat à l'Energie Atomique, University of Grenoble Alpes, MINATEC Campus, Grenoble 38040, France; alexis.abraham@cea.fr (A.A.); Thomas.anfray@cea.fr (T.A.); olivier.dubray@cea.fr (O.D.); daivid.fowler@cea.fr (D.F.); segolene.olivier@cea.fr (S.O.)

[2] Centre de Nanosciences et de Nanotechnologies (C2N), Université Paris Sud, CNRS, Université Paris Saclay, Orsay 91405, France; delphine.morini@u-psud.fr

* Correspondence: benoit.charbonnier@cea.fr; Tel.: +33-4-38-78-0162

Academic Editor: Paolo Minzioni
Received: 21 October 2016; Accepted: 23 November 2016; Published: 29 November 2016

Abstract: Optical modulators are key components to realize photonic circuits, and Mach-Zehnder modulators (MZM) are often used for high speed short reach interconnects. In order to maximize the tolerable path loss of a transmission link at a given bitrate, the MZM needs to be optimized. However, the optimization can be complex since the overall link performance depends on various parameters, and, for the MZM in particular, implies several trade-offs between efficiency, losses, and bandwidth. In this work, we propose a general and rigorous method to optimize silicon MZM. We first describe the optical link, and the numerical method used for this study. Then we present the results associated to the active region for 1310 nm applications. An analytical model is generated, and allows us to quickly optimize the p-n junction depending of the targeted performances for the MZM. Taking into account the required optical link parameters, the maximum tolerable path losses for different length of MZM is determined. By applying this method, simulations show that the optimum MZM length for 25 Gbps applications is 4 mm with an efficiency of 1.87 V·cm, 0.52 dB/mm of losses. A tolerable path loss of more than 25 dB is obtained.

Keywords: silicon photonics; Mach-Zehnder Modulators; optical communictions; short reach Interconnects

1. Introduction

Silicon photonics is known as a promising platform for high speed applications, and in recent years, the maturity of the technology has allowed the proposal of photonic chips with the necessary components [1–4]. Even if several investigations are still ongoing [5], silicon Photonics is now a proven technology for high speed short reach optical interconnects with several companies proposing 100GBASE compatible products [6–8]. As data rates increase from 10 G to 25 G to 100 G per wavelength [9], the design of these optical links relies on a careful balance between several parameters such as for instance the receiver sensitivity, the modulator efficiency or the laser power. This balance depends upon many system level parameters (e.g., tolerable link loss) but also technological parameters (e.g., doping levels of the active regions) and external constraints (e.g., power consumption). In this paper, we focus on the Mach-Zehnder Modulator (MZM) used in such links, operating at 1310 nm, and propose a method to optimize its technological and physical parameters independently of the other system building blocks.

Based upon the plasma dispersion electro-optical effect, the active region of the modulator creates a phase shift, which is then converted into an intensity modulation by using an interferometric

structure. In order to obtain the best specifications for a targeted application, a compromise between insertion loss, modulation bandwidth and efficiency must be found. This optimal point is difficult to obtain without a proper method or compact model, because it depends on various parameters. In a previous work, we bypassed this issue by developing a compact model for the conception of a ring modulator in order to find the optimal point in the most general case [10]. This paper completes this discussion by detailing a similar method to obtain the best parameters for the MZM, which we apply to short reach interconnects, with 25 Gbps On-Off Keying (OOK) modulation at 1310 nm. The objective of this study is thus to determine the configuration of the MZM which leads to the largest tolerable path loss for the overall link, and see the reachable performances for the modulator.

The article is divided into three sections. The notations and the main elements referred to in the optimization procedure are explained in the first part. In the second part, after having determined the required power for the receiver, the electro-optical performance parameters of the active region of the MZM are extracted, including bandwidth simulations. The compact model for the optimal parameters of the junction is also presented. Last, the third part details the optimization method through one example, and combines all the previous data to optimize the MZM in a more general case.

2. Notations and Methodology

2.1. Presentation of a Typical High Speed Short Reach Interconnect

The structure of a high speed short reach interconnect is presented schematically in Figure 1. It is made of a laser source hybridized to a Silicon Photonic circuit with a fiber coupled to the output port. In a Space Division Multiplexing (SDM) configuration, usually, a single laser source is split onto parallel MZM based transmit circuits, each is coupled to an individual output single polarization grating coupler (SPGC). On the receiver side, individual input Polarization Splitting Grating Coupler (PSGC) are directly connected to parallel receiver circuits. In a dual fiber configuration using Wavelength Division Multiplexing (WDM), the transmitter silicon photonic circuit consists of a number of MZM connected to individual laser sources on one side and, on the other side, to a wavelength multiplexer followed by a SPGC. The corresponding receiver consists of an input PSGC followed by a wavelength de-multiplexer and parallel receiver circuits.

We consider as variables only the input optical power feeding the MZM, P_{LAS} and the parameters defining the MZM that we aim to optimize. These are the insertion loss of the doped electrodes $\mathrm{IL}_{\mathrm{MZM}}$, the modulation efficiency measured as the half wave voltage V_{π}, and the electro-optic bandwidth $\mathrm{BW}_{\mathrm{MZM}}$. As we aim at maximizing the tolerable path loss, the laser relative intensity noise contribution to the link performance is assumed to be negligible and thus the laser source is considered perfect.

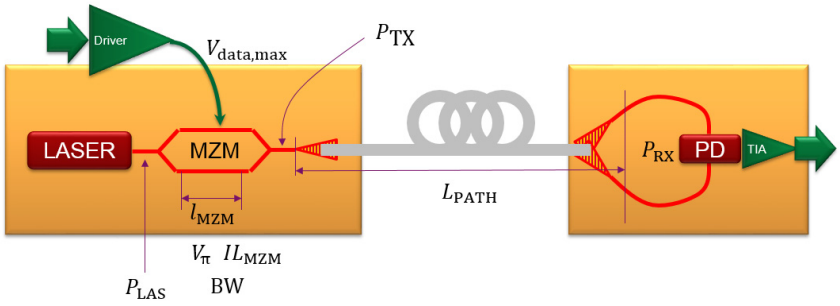

Figure 1. Simplified schematic of a high speed short reach link with the parameters used in the simulation. MZM: Mach-Zehnder Modulator; PD: Photo-Detector.

At the MZM output, these parameters leads to a given average optical output power P_{TX} and extinction ratio ER or Optical Modulation Amplitude (OMA). Based on these output parameters and on the link configuration ($\mathrm{IL}_{\mathrm{PATH}}$, which is a sum of the multiplexing, fiber coupling and fiber losses),

the average power reaching the photodetectors is denoted P_{RX}. Note that the chromatic dispersion of the link, which is assumed to be operated around 1.3 µm, is considered negligible. Different photodetector parameters will lead to a given sensitivity i.e., the minimum power required, when the input optical signal is "perfect", to reach a Bit Error Rate (BER) better than 10^{-9}. This parameter is denoted P_{SEN}. In our case, as the signal reaching the photo-receiver will not be ideal (for instance, it may exhibit a low ER), the input power required to reach a BER < 10^{-9} will be larger than P_{SEN}. Let us denote this value P_{REQ}.

We aim to identify the best choice of the MZM parameters $\left[\begin{array}{ccc} IL_{MZM} & V_\pi & BW_{MZM} \end{array}\right]$ that maximizes the optical budget IL_{PATH} that the system can accommodate i.e., the difference between P_{TX} and P_{REQ}. In order to be more realistic, this optimization will be made under the constraint that the RF driving amplitude of the MZM is equal to $V_{data} = 2.4$ V and that the MZM is driven either in single drive or in dual drive configuration (with $1/2 \times V_{data}$ on each arm). With our simplified model, the single ended and push-pull operation of the MZM are equivalent to one another.

2.2. Simulation of the Input Power Required P_{REQ}

In a first step, we determine the input power required P_{REQ} as a function of the MZM parameters $\left[\begin{array}{cc} V_\pi & BW_{MZM} \end{array}\right]$ by using a split-step Fourier based simulator [11] running in Matlab® (R2015b, Mathworks, Natick, MA, USA). At this stage we do not consider that there is a link between V_π and BW_{MZM} in order to map the complete parameter space even if, as a result, some simulated MZM do not represent realistic situations. A transmission link at a data rate of 25 Gbps comprising a perfect continuous laser source followed by a MZM with a given V_π and BW_{MZM} is modelled. A variable optical attenuator is then used prior to the photo-receiver to vary the optical input power P_{RX}, simulating the passive optical losses IL_{PATH}. The photo-receiver (RX) itself consists of a PIN photodiode with responsivity $\eta_{OE} = 0.9$ A/W, analogue bandwidth $BW_{PD} = 21$ GHz, a Trans-Impedance Amplifier (TIA) gain of 1 kΩ and a Noise Equivalent Power (NEP) of 8 pW/$\sqrt{}$GHz. These RX parameters are typical for 25 Gbps systems [12] and, as will be evident later, do not change the generality of the results or of the proposed method. The transmission quality is evaluated by means of the Q-factor with patterning effects of the two nearest neighboring bits being taken into account in the calculation [13]. Note that a Q factor of 6 corresponds to a BER of 10^{-9}.

With the parameters given above, we first find that P_{SEN} is equal to −20.8 dBm at 25 Gbps. Figure 2 shows the required power P_{REQ} computed by simulation as a function of V_π and BW_{MZM} for an absolute voltage V_{data} of 2.4 V.

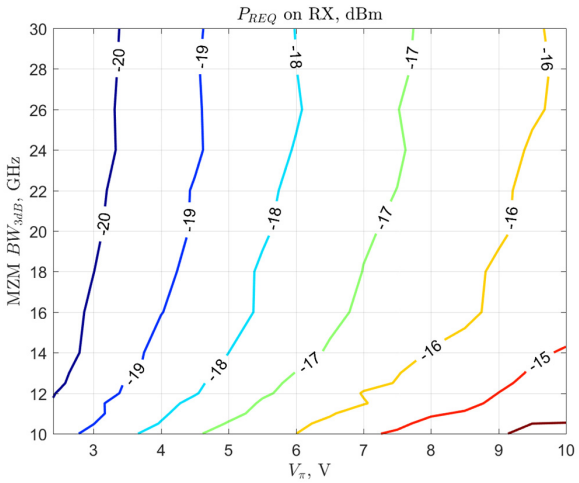

Figure 2. Evolution of the required receiver input for 25 Gbps On-Off Keying (OOK) modulation depending of the voltage and the electro-optic bandwidth of the Mach-Zehnder modulator (MZM). The receiver parameters are defined in the text.

For the smallest value of V_π and the largest value of BW_{MZM} considered (2.4 V and 30 GHz respectively), we find that $P_{REQ} = P_{SEN} = -20.8$ dBm as may be expected as the transmitter emits a "perfect" signal. When V_π increases (thus decreasing the extinction ratio) or when BW_{MZM} decreases (thus closing the eye diagram), the value of P_{REQ} increases. This graph allows us to consider the different possible trade-offs between the three MZM key parameters $\left[\begin{array}{ccc} IL_{MZM} & V_\pi & BW_{MZM} \end{array} \right]$ as IL_{MZM} directly impacts the RX input power.

2.3. EO Performances of the Active Region of the MZM

Silicon MZM electro-optical performances such as loss and modulation efficiency are more often referred to in terms of unit length: the loss α in (dB/mm), and the phase modulation efficiency between 0 V and V_π noted as $\Delta\varphi$ in ($^\circ$/mm). The later parameter is linked to the product $V_\pi L_\pi$ in (V·cm) with the relation:

$$\Delta\varphi = \frac{360 \times \Delta n_{eff}}{\lambda} = \frac{180 \times V_\pi}{V_\pi L_\pi} \quad (1)$$

When the MZM electrode length l_{MZM} is set, we can write $IL_{MZM} = \alpha \times l_{MZM}$. Since the voltage V_π represents the voltage needed for a given length l_{MZM} to obtain a shift of π, for an estimated efficiency of $V_\pi L_\pi$ we have also the relation $V_\pi = V_\pi L_\pi / l_{MZM}$. Several phase shifting mechanisms exist [14] and give different compromises between these two parameters. In our case, we choose a doped p-n junction working in the depletion regime since it is currently the most common type used for high speed silicon modulators. The junction is embedded in a rib waveguide of 400 nm of width, 300 nm of height, and with a slab of 150 nm of height. In order to illustrate what may be achieved in terms of $V_\pi L_\pi$ and α for this junction, a parametric study was performed depending on the doping level of the N and P sides between (6.10^{16}–5.10^{18}) cm^{-3}, which is the order of magnitude of the doping levels using in the PN modulators. The doping levels impact the depletion width, and thus the capacitance of the p-n junction (see Section 2.4). The doping regions are assumed to have uniform doping densities and the junction is perfectly vertical. The performances of the modulator at 1310 nm and at an absolute bias voltage of 2.4 V are obtained by electro-optical simulations using Lumerical® software (2016a, Lumerical Solutions Inc., Vancouver, BC, Canada). The refractive indices of the materials were $n_{Si} = 3.48$, and $n_{SiO2} = 1.44$, and the Soref equations at 1310 nm were used [15]. Since the undoped propagation loss is mainly dominated by side wall roughness and thus is a foundry parameter, it is not included in the simulations in order to keep a more general approach. This variable is implicitly included in the tolerable path loss. The optimal position of the junction inside the waveguide, noted δ_{PN} and represented Figure 3, ensuring the best efficiency for each couple of doping N_A and N_D is implicitly included in the simulation. This offset can be obtained numerically by using a 1D model under the assumptions that: (1) the refractive index variations are induced by an abrupt p-n junction (equivalent of two correlated rectangular functions), and (2) at half height of the waveguide, the optical mode profile can be fitted by a center Gaussian profile with a beam's width σ of 87 nm for a waveguide of 400 nm of width at 1310 nm. The optimal position corresponds to the maximum of the convolution product between the two functions.

Figure 3 displays the possible couples of efficiency and loss of the active region for all the doping levels simulated (purple region). The ideal MZM would have a small value of α and large $\Delta\varphi$, however simulations show that it is not possible to decrease one without decreasing the other. The unavoidable compromise between α and $V_\pi L_\pi$ expresses the intrinsic limitation of the junction itself. The best compromises are represented on the blue dash line on the graph. This curve is crucial for the design of optical modulator since it includes all the parameters of the p-n junction which allows us to obtain the best compromise between the efficiency and the losses.

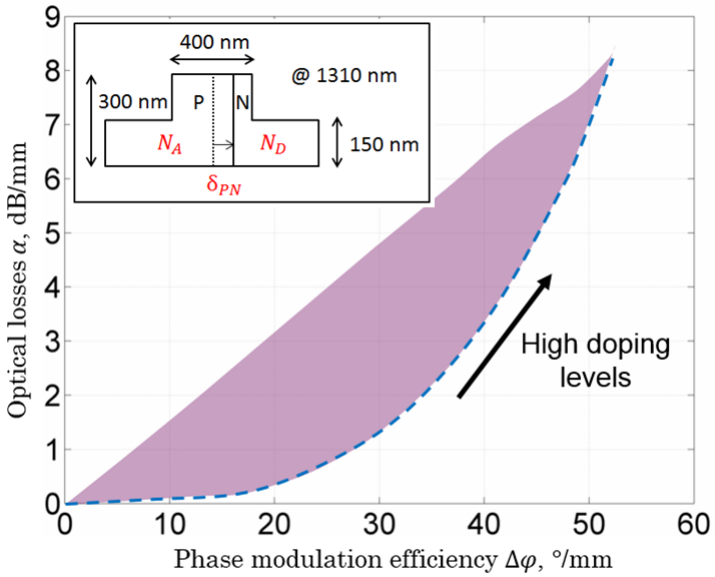

Figure 3. Diagram of optical losses as a function of the phase shift for an absolute bias voltage of 2.4 V at 1310 nm. The purple area includes all the simulated couples of doping level. The dash blue curve is the best case described by the Equation (3).

We find that it is possible to fit the dash blue curve with polynomial functions, leading to simple relationships between α_{MZI}, $\Delta\varphi$, δ_{PN} and the doping concentrations N_A and N_D (Equations (2)–(5)) for the structures showing the best compromises between efficiency and losses for an efficiency up to $20°/\mathrm{mm}$.

$$\alpha_{\mathrm{MZI}}\,[\mathrm{dB/mm}] = 6.68 \times 10^{-4}\Delta\varphi^2 - 2.51 \times 10^{-1}\Delta\varphi + 2.84 \quad (2)$$

$$10\log(N_D\,[\mathrm{cm}^{-3}]) = -2.89 \times 10^{-4}\Delta\varphi^2 + 5.37 \times 10^{-2}\Delta\varphi + 16.43 \quad (3)$$

$$10\log(N_A\,[\mathrm{cm}^{-3}]) = -4.32 \times 10^{-4}\Delta\varphi^2 + 7.14 \times 10^{-2}\Delta\varphi + 15.79 \quad (4)$$

$$\delta_{\mathrm{PN}}\ (\mathrm{nm}) = -15.61 \times 10^{-5}\Delta\varphi^4 - 29.18 \times 10^{-3}\Delta\varphi^3 + 20.45 \times 10^{-1}\Delta\varphi^2 - 64.52 \times \Delta\varphi + 800.88 \quad (5)$$

Figure 4 provides a graphic interpretation of the fitted relations compared to the simulated points. It allows a quick access of all parameters of the active region. The electro-refraction effect is more important for holes than for electrons in this range of doping levels, and since the depletion variation is always more important in the less doped region, a larger variation of concentration of holes is obtained when $N_A < N_D$. In order to place this variation close to the center of the waveguide (where the maximum of the optical power is located), the position of the p-n junction is shift towards the n-doped side, so we have $\delta_{\mathrm{PN}} > 0$. Finally, the magnitude of the electro-optical effect is directly correlated with the amplitude of the carrier variations, high modulation efficiency implies high doping levels. However the depletion width is then reduced, so the position of the p-n junction will be closer to the center of the waveguide (δ_{PN} decrease).

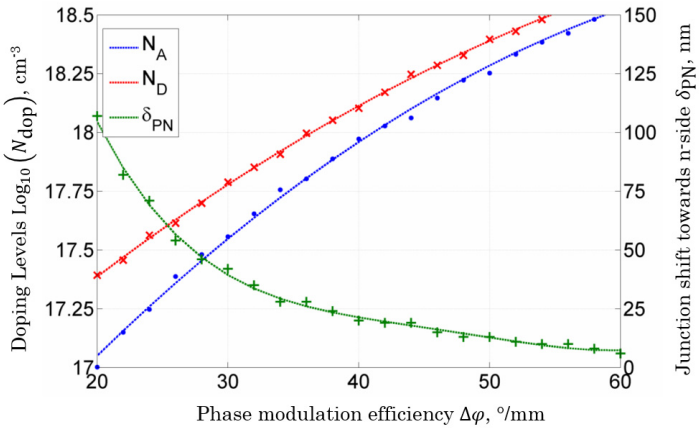

Figure 4. Evolution of the doping concentrations and the position of the p-n junction in function of the targeted efficiency for the simulated active region. Symbols are the results of Lumerical simulations, lines are polynomial fits.

2.4. Modulation Bandwidth

The modulation bandwidth is also a figure of merit that must be taken into account in the conception of the MZM. Indeed, the longer the MZM electrode is, the higher its direct current (DC) modulation efficiency is but the smaller its radio-frequency (RF) bandwidth is. Figure 5 shows a simulation of the 3 dB RF bandwidth for an absolute bias voltage of 2.4 V of the electrical S21 parameter of the electrode itself as a function of its length for typical implantation and metallization conditions (detailed later). For these simulations we use an analytical equivalent circuit model for the traveling wave electrode which drives the carrier depletion silicon MZM. The model is composed of an elementary lossy dispersive transmission line (LDTL) model of length ∂l which is cascaded to fully represent the length of the electrode l_{MZM}. The elementary LDTL model, depicted on Figure 6, includes frequency dependent resistors, capacitors and inductors. This model addresses two of the three factors that determine the operation speed of a traveling wave electrode MZM: (i) the microwave attenuation; (ii) the impedance matching; but do not take into account the velocity matching between the RF and the optical waves. However Hui Yu et al. proves that velocity mismatching does not limit the electrode bandwidth for electrode of reasonable length compared to the RF loss and the impedance mismatching effects [16]. The series resistor and inductor R_{metal} and L_{metal} are frequency dependent and their formulas are given in [17]. All the other elements except the PN junction capacitance ($C_{junction}$) and the access resistor (R_{access}) are computed similarly as in [16]. The junction capacitance is computed as in [18] and takes into account the fringing field effect. The access resistor is extracted from measurements on our fabrication platform.

The simulation results depicted on Figure 5 have been obtained using a SPICE simulator (AMS 16.1, MENTOR Graphics, Wilsonville, OR, USA). We took a coplanar line with 200 µm-width grounds, 10 µm-width signal and 22.5 µm-space between them. The substrate, the buried oxide and the optical guide (ribbon) heights are respectively 800 µm, 2 µm and 300 nm. The metallization thickness is 1.3 µm. Doping concentrations for p and n part of the junction are both 2.5×10^{17} cm^{-3}. As we expected, the shorter the length of the electrode is, the higher the bandwidth is. This is mainly due to the decrease of the RF loss. Ultimately the bandwidth will be limited by the doped-silicon access resistor and the junction capacitance. For very short electrode lengths, under 500 µm, we can expect very high bandwidths up to 50 GHz. These results illustrate from another viewpoint the possible tradeoff between MZM parameters.

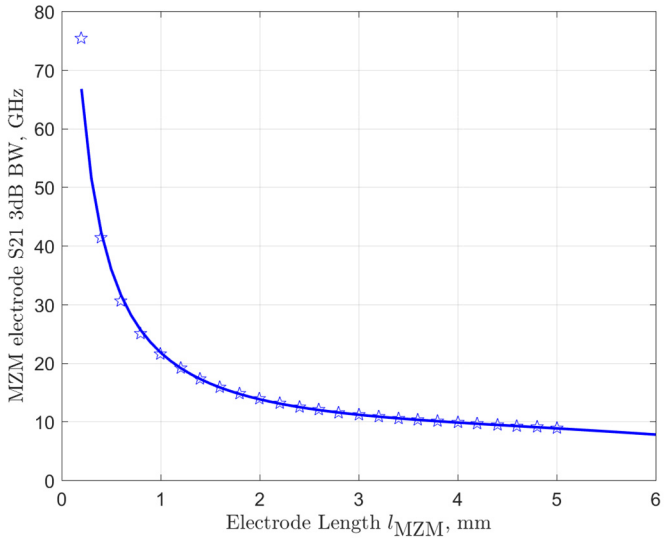

Figure 5. MZM electrical modulation bandwidth vs. electrode length. Symbols are simulation results and the line is a polynomial fit to those results.

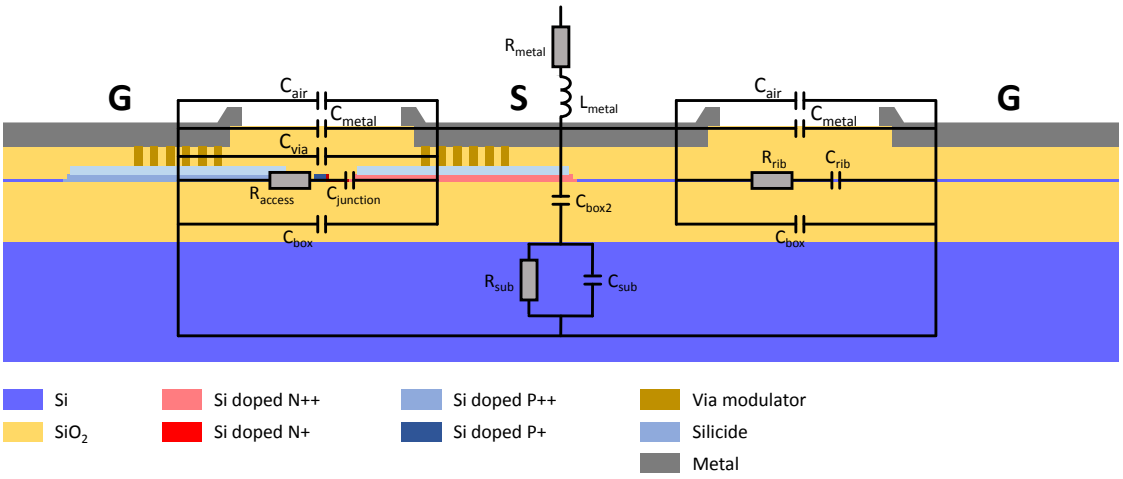

Figure 6. MZM Transmission line equivalent circuit model.

3. MZM Parameter Optimization

The optimization of the MZM parameters $\begin{bmatrix} \mathrm{IL_{MZM}} & V_\pi & \mathrm{BW_{MZM}} \end{bmatrix}$ is equivalent to the optimization of $\begin{bmatrix} \alpha_{\mathrm{MZM}} & \Delta\varphi & l_{\mathrm{MZM}} \end{bmatrix}$ due to the relationship between these parameters as described in the section above. In order for a MZM with given parameters to be compliant with the transmission performance required, it must satisfy the condition $P_{\mathrm{RX}} \geq P_{\mathrm{REQ}}$, where (in dB scale):

$$P_{\mathrm{RX}} = P_{\mathrm{LAS}} - \alpha_{\mathrm{MZM}} \times l_{\mathrm{MZM}} - 3 - \mathrm{IL_{PATH}} \tag{6}$$

The 3 dB term accounts for the fact that the MZM is biased in quadrature. The target value of P_{REQ} is determined form Figure 2 with $V_\pi = (V_\pi L_\pi)/l_{\mathrm{MZM}}$, and the bandwidth value $\mathrm{BW_{MZM}}$ is taken from Figure 5.

In order to illustrate the optimization process, we arbitrarily set the value of $P_{\mathrm{LAS}} = +10$ dBm and the MZM length $l_{\mathrm{MZM}} = 1$ mm. Figure 7 shows the limiting curves in the $\begin{bmatrix} \alpha_{\mathrm{MZM}} & V_\pi L_\pi \end{bmatrix}$

space. The upper limit (blue curve) is linked to the requirement described above i.e., the highest MZM insertion loss that satisfies $P_{RX} \geq P_{REQ}$ when $IL_{PATH} = 0$:

$$\alpha_{MZM} \leq (P_{LAS} - 3 - P_{REQ}) / l_{MZM} \quad (7)$$

where P_{REQ} is also a function of V_π and BW_{MZM} or, in other terms, of α_{MZM} and $V_\pi L_\pi$. The thick blue curve is extracted directly from the numerical results of Figure 2 while the dashed thin blue line is an analytical extrapolation of these results for large V_π. When V_π increases, the eye diagram closes and a power penalty related to the degraded extinction ration is subtracted to the tolerable link budget, thus reducing the allowed MZM insertion loss. The thick black line shows the lower limit with the best performing MZM (Figure 3) based on our simulated waveguide and junction geometry. All the MZM within those two limits offer sufficient performances for a 25 Gbps link to operate with a BER < 10^{-9}. However, the MZM whose parameters are situated on the upper limit (blue dashed line) have the maximum allowable insertion loss and thus do not permit additional losses to be inserted between the TX and RX (i.e., $P_{RX} = P_{REQ}$ for those parameters).

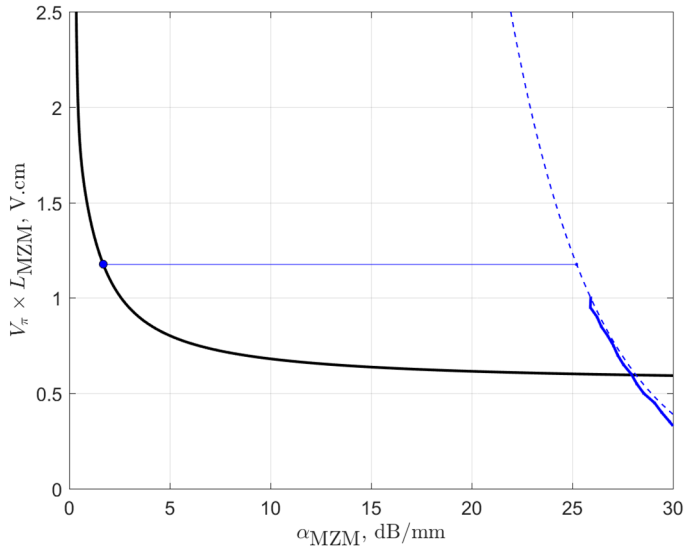

Figure 7. MZM Parameter space limits: upper limit linked to insertion loss (**blue**); and lower limit due to technology (**black**). $l_{MZM} = 1$ mm.

On the contrary, the MZM whose parameters are situated on the black line offer the best performance in terms of efficiency and insertion loss and lead to the availability of path loss margin. Among all the possible parameters $\begin{bmatrix} \alpha_{MZM} & V_\pi L_\pi \end{bmatrix}$ belonging to this lower limit, one particular point maximizes the optical loss L_{PATH} that can be tolerated between the transmitter (TX) and receiver (RX), this point is represented by a blue dot on Figure 7 at 1.7 dB/mm and 1.17 V·cm. Indeed, if we draw a horizontal line from this optimal point to the upper limit curve, the intersect point is situated at 25.2 dB/mm and 1.17 V·cm. The loss that can be tolerated is thus $(25.2 - 1.7) \times l_{MZM} = 23.5$ dB with a MZM length of 1 mm. For clarity, we plot on Figure 8 the tolerable path loss as a function of $V_\pi L_\pi$ directly computed from Figure 7 i.e., the difference along the x-axis between the black and dash-blue curves of Figure 7 multiplied by the MZM length.

In summary, for a 1 mm long MZM, the optimal parameters are $V_\pi = 11.7$ V and $IL_{MZM} = 1.7$ dB which leads to an electrical bandwidth of $BW_{MZM} = 23.5$ GHz and a system optical budget of $IL_{PATH} = 23.5$ dB for an input laser power $P_{LAS} = +10$ dBm. If a MZM with higher modulation efficiency was used (further to the right on the black line), the improvement in extinction ratio would not be sufficient to compensate the inevitable higher insertion loss and thus, the tolerable path loss would decrease. The reverse applies if we considered a MZM with lower insertion loss. It is important

to underline that the optimal parameters found above are valid whatever the sensitivity of the receiver or the laser power. Indeed, if the RX sensitivity is degraded or the laser power is lowered, the tolerable path loss decreases (translation along the x-axis of the blue curve) but the optimal MZM parameters do not change.

This optimization can be repeated for different values of l_{MZM} in order to find the optimal electrode length (Figure 9). We plot in Figure 10 the evolution of the maximum $\mathrm{IL}_{\mathrm{PATH}}$ as a function of l_{MZM}. The optimum MZM electrode length is found to be 4 mm, which leads to $\alpha_{\mathrm{MZM}} = 0.52$ dB/mm and a product $V_\pi L_\pi$ of 1.87 V·cm at -2.4 V ($\Delta\varphi = 23°/\mathrm{mm}$) or, in other terms, $V_\pi = 4.6$ V and $\mathrm{IL}_{\mathrm{MZM}} = 2.1$ dB. For a laser power $P_{\mathrm{LAS}} = +10$ dBm and a receiver sensitivity $P_{\mathrm{SEN}} = -20.8$ dBm at 25 Gbps, we find a tolerable path loss $\mathrm{IL}_{\mathrm{PATH}} = 25.9$ dB.

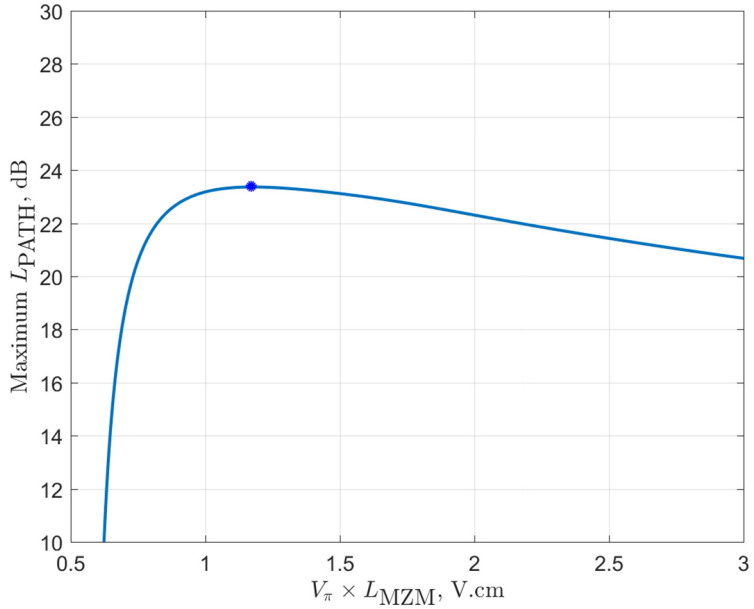

Figure 8. Maximum tolerable path loss as a function of $V_\pi l_{\mathrm{MZM}}$ for $l_{\mathrm{MZM}} = 1$ mm.

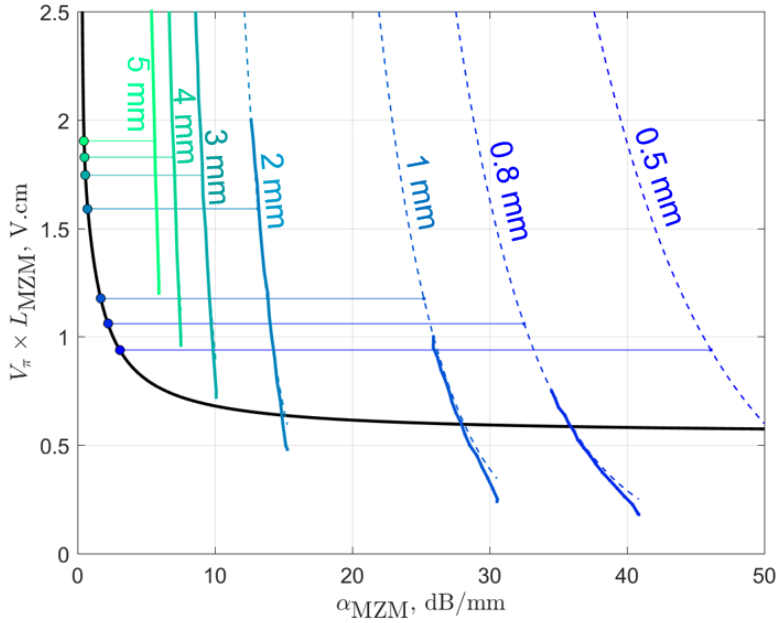

Figure 9. MZM optimal parameter search for different electrode lengths.

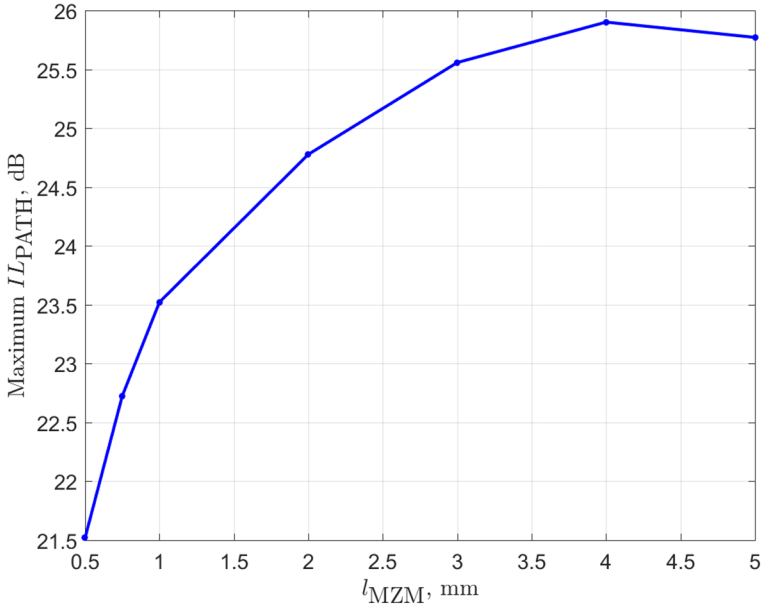

Figure 10. Maximum tolerable path loss as a function of MZM electrode length.

4. Conclusions

In conclusion, we propose an optimization method for the design of MZMs maximizing the tolerable path loss of the optical link for high speed short reach optical interconnects. This optimization is based on the best compromise between the efficiency and the losses of the active region. This compromise is independent from the laser power used and receiver sensitivity. A compact model allows us to have an easy correspondence between the EO-performances and the parameters of the p-n junction. In the case of 25 Gbps OOK modulation at 1310 nm, simulations show a MZM of 4 mm is optimal with an efficiency of 23.1°/mm at −2.4 V.

The next step is to validate this approach by an experimental characterization of MZM. For more investigations, this method can be easily adapted for different types of active regions, by taking into account the fabrication effects such as implantation conditions, or for more complex modulation formats and other symbol rates.

Acknowledgments: The research leading to these results has received funding from the French national program "programme d'Investissements d'Avenir, IRT Nanoelec" referenced ANR-10-AIRT-05.

Author Contributions: A.A., O.D., D.M.-M. and S.O. mainly contributed to the optimization of the MZM junction and modelling of the doping implantation. T.A. contributed to the RF modelling of the MZM electrodes. B.C. and D.F. devised the optimization methodology and system level simulations. All authors participated actively in the writing of this paper.

Conflicts of Interest: The authors declare no conflict of interest.

References

1. Bernabe, S.; Charbonnier, B.; Blampey, B.; Malhouitre, S.; Castany, O.; Temporiti, E.; Minoia, G.; Baldi, G.; Repossi, M.; Pares, G.; et al. A fully packaged 25 Gbps/channel WDM photoreceiver module based on a Silicon Photonic Integrated Circuit and a flip-chipped CMOS quad Transimpedance Amplifier. In Proceedings of the IEEE Optical Interconnects Conference (OI), San Diego, CA, USA, 9–11 May 2016.
2. Sun, C.; Wade, M.T.; Lee, Y.; Orcutt, J.S.; Alloatti, L.; Georgas, M.S.; Waterman, A.S.; Shainline, J.M.; Avizienis, R.R.; Lin, S.; et al. Single-chip microprocessor that communicates directly using light. *Nature* **2015**, *528*, 534–538. [CrossRef] [PubMed]

3. Milivojevic, B.; Wiese, S.; Anderson, S.; Brenner, T.; Webster, M. Demonstration of Optical Transmission at Bit Rates of up to 321.4 Gb/s using Compact Silicon Based Modulator and Linear BiCMOS MZM Driver. In Proceedings of the Optical Fiber Communications Conference, Anaheim, CA, USA, 20–24 March 2016.
4. Temporiti, E.; Minoia, G.; Repossi, M.; Baldi, D.; Ghilioni, A.; Svelto, F. A 56 Gbps 300 mW Silicon-Photonics Transmitter in 3D-Integrated PIC25G and 55 nm BiCMOS Technologies. In Proceedings of the International Solid-State Circuit Conference (ISSCC), San Francisco, CA, USA, 31 January–4 February 2016.
5. Thomson, D.; Zilkie, A.; Bowers, J.; Komljenovic, T.; Reed, G.; Vivien, L.; Marris-Morini, D.; Cassan, E.; Virot, L.; Fédéli, J.M.; et al. Roadmap on silicon photonics. *J. Opt.* **2016**, *18*. [CrossRef]
6. Mellanox MFS1200-xxxx. Available online: www.mellanox.com (accessed on 19 October 2016).
7. Luxtera LUX42604 QSFP. Available online: www.luxtera.com (accessed on 19 October 2016).
8. Intel SPTSBPxCLCDF. Available online: www.intel.com (accessed on 19 October 2016).
9. IEEE802.3ba: 40 Gb/s and 100 Gb/s Ethernet Task Force. Available online: http://www.ieee802.org/3/ba/ (accessed on 19 October 2016).
10. Dubray, O.; Abraham, A.; Hassan, K.; Marris-morini, D.; Vivien, L.; Connor, I.O.; Menezo, S. Electro-Optical Ring Modulator: An Ultracompact Model for the Comparison and Optimization of pn, pin, and Capacitive Junction. *IEEE J. Sel. Top. Quantum Electron.* **2016**, *22*, 1–10. [CrossRef]
11. Watkins, L.R.; Zhou, Y.R. Modelling Propagation in Optical Fibers Using Wavelets. *IEEE J. Lightwave Technol.* **1994**, *12*, 1536–1542. [CrossRef]
12. Boeuf, F. Recent progress in Silicon Photonics R&D and manufacturing on 300 mm wafer platform. In Proceedings of the Optical Fiber Conference, Los Angeles, CA, USA, 22–26 March 2015.
13. Mattera, F.; Settembre, M. Role of Q-factor and of time jitter in the performance evaluation of optically amplified transmission systems. *IEEE J. Sel. Top. Quantum Electron.* **2000**, *6*, 308–316. [CrossRef]
14. Reed, G.T.; Mashanovich, G.; Gardes, F.Y.; Thomson, D.J. Silicon optical modulators. *Nat. Photonics* **2010**, *4*, 518–526. [CrossRef]
15. Soref, R.; Bennett, B. Electrooptical effects in silicon. *IEEE J. Quantum Electron.* **1987**, *23*, 123–129. [CrossRef]
16. Yu, H.; Bogaerts, W. An Equivalent Circuit Model of the Traveling Wave Electrode for Carrier-Depletion-Based Silicon Optical Modulators. *IEEE J. Lightwave Technol.* **2012**, *30*, 1602–1609. [CrossRef]
17. Heinrich, W. Quasi-TEM Description of MMIC Coplanar Lines Including Conductor-Loss Effects. *IEEE Trans. Microw. Theory Tech.* **1993**, *41*, 45–52. [CrossRef]
18. Jayatilleka, H.; Sacher, W.D.; Poon, J.K.S. Analytical Model and Fringing-Field Parasitics of Carrier-Depletion Silicon-on-Insulator Optical Modulation Diodes. *IEEE Photonics J.* **2013**, *5*. [CrossRef]